Supporting Online Material for

The Onset of Turbulence in Pipe Flow

Kerstin Avila,* David Moxey, Alberto de Lozar, Marc Avila, Dwight Barkley, Björn Hof*

*To whom correspondence should be addressed. E-mail: kavila@ds.mpg.de (K.A.); bhof@ds.mpg.de (B.H.)

Published 8 July 2011, *Science* **333**, 192 (2010)
DOI: 10.1126/science.1203223

This PDF file includes:

Supporting Online Material for

The onset of turbulence in pipe flow

Kerstin Avila, David Moxey, Alberto de Lozar,
Marc Avila, Dwight Barkley and Björn Hof
correspondence to: kavila@ds.mpg.de, bhof@ds.mpg.de

This PDF file includes:

Materials and Methods
Figures S1 - S5
Tables S1- S3

1 Materials and Methods

Numerical Simulations

The numerical results presented here have been obtained with two distinct methods. The first (DNS1) is the spectral-element–Fourier code *Semtex* (*1*), which solves the Navier–Stokes equations in Cartesian coordinates (x,y,z). 36 spectral elements are used to represent the circular (y,z) cross-sections of a pipe. Elements are placed to mimic the radial distribution of Chebyshev collocation points, with fields approximated using a 12th order polynomial expansion basis within each element. Fourier modes are used in the periodic axial direction at a density of 768 complex modes (1536 collocation points) per $100D$ in pipe length.

The second (DNS2) is the hybrid spectral finite-difference method of (*2*), which solves the equations in cylindrical coordinates (x,r,θ). The numerical discretization consists of a non-equispaced 9-point finite-difference stencil in r and of Fourier modes in θ and z. Here 56 radial points, ± 32 azimuthal Fourier modes and ± 1024 axial Fourier modes (64 and 2048 collocation points, respectively) have been used per $L = 32\pi D \simeq 100D$ in pipe length.

Both methods use periodic boundary conditions in the streamwise direction, fix the diameter at $D = 1$, and impose constant volume flux (so that $U = 1$), ensuring no variation in Re (which is given by $1/\nu$), during any run.

Initial conditions for ensemble runs where obtained from snapshots of simulation of puffs at lower Re, similarly to the approach in puff lifetime studies (*3*). In the case of the spectral-element–Fourier (DNS1) runs, all such initial conditions were generated from simulations at $Re = 2100$ with snapshots taken every 20 (D/U). In the case of the hybrid spectral finite-difference (DNS2) runs, all such initial conditions were generated from simulations at $Re = 2200$ with snapshots taken every 10 (D/U).

Experiments: Pressure measurements

Pressure measurements are performed at two positions along the pipe. The first measurement is made $50D$ downstream of the perturbation in order to verify the generation of a single puff by the perturbation. The second one is located at various distances $L > 50D$ from the perturbation in order to determine the subsequent turbulent fraction. Sensors measure the pressure difference over $3D$ along the pipe. Pressure sensors are connected via tubes to pressure taps in the pipe wall as illustrated in Fig. S1. We used the low pressure sensor DP45 from Validyne with the diaphragm no. 14 (0.021 - 0.049 PSI). Special care was taken to remove all airbubbles from the tubes and sensor prior to measurements. Such air pockets could alter the signal and even reinduce disturbances into the pipe under unsteady flow conditions.

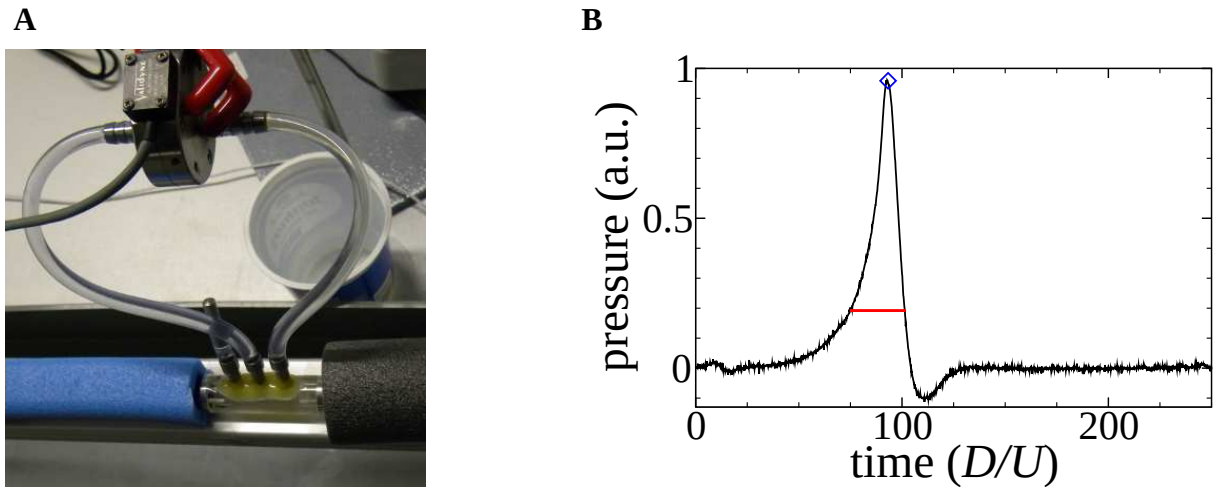

Figure S 1: Pressure difference measurement at a machined perspex connector. **(A)** The connector features three holes of $0.2D$ diameter and separated by $3D$, of which here two neighboring ones are used for the pressure measurement. Air bubbles are removed from the sensor and the tubing prior to usage. The precision glass tube to the left and right are covered by insulating materials to minimize temperature effects and light exposure (to avoid algae growth). **(B)** The pressure signals are then analyzed to detect the number of peaks (here one, marked by the blue diamond) and the length of the turbulent region at 20% of the maximal pressure peak, indicated by the red line.

Puff speed

To convert between distances and times and to plot puffs in co-moving frames of reference, We use the following approximation for the Reynolds number dependent puff speed:

$$U_p = 1.482 - 2.416 \times 10^{-4} Re \tag{1}$$

This is shown graphically in Fig. S2.

Obtaining confidence intervals for DNS

As seen in table S3, each observed lifetime $t_1, \ldots, t_n$ obtained through DNS is censored by imposing an upper bound on the simulation time so that $t_i \leq t_{\max}$. In (*4*) this is defined as type I censoring, for which exact confidence intervals do not exist and must therefore be approximated numerically. Given the small number of samples, the central limit theorem provides inaccurate intervals, and so here we opt to use the technique of *bootstrapping* as seen in appendix D.2 of (*4*). The procedure for generating confidence intervals is as follows:

1. Generate a pseudorandom sample $t_1^*, t_2^*, \ldots, t_n^*$ by sampling from the set of lifetimes with replacement.

2. Calculate the maximum likelihood estimator $\hat{\tau}_1^*$ of this data as

$$\hat{\tau}_1^* = \frac{1}{r_1^*} \sum_{k=1}^{n} t_k^*,$$

where r_1^* is the number of uncensored lifetimes and $t_0 + t_k^* = t_{\max}$.

3. Repeat the previous two steps B times to obtain bootstrap samples $\{\hat{\tau}_1^*, \hat{\tau}_2^*, \ldots, \hat{\tau}_B^*\}$.

4. Sort this data so that $\hat{\tau}_b^* \leq \hat{\tau}_{b+1}^*$.

Assuming $B = 10^k$ where $k \geq 2$, confidence intervals at level $1-\alpha$ may then be read off as $[\hat{\tau}_{B\alpha/2}^*, \hat{\tau}_{B(1-\alpha/2)}^*]$.

Analysis of the experimental data

The analysis of each set of experimental measurements leads to a splitting probability $P(Re, L) = r/n$. Here L is the downstream distance from the perturbation and r is the number of runs that splitted out of a total of n (see Table 1). In the first step L is converted into time t by using the puff speed approximation of equation (1). The mean time τ of the splitting process with formation time $t_0 = 100$ is then caclulated as:

$$\tau = \frac{t_0 - t}{\log(1 - P(Re, t))} \tag{2}$$

The 95% confidential intervals P (shown in Figure 4 of the paper) are estimated by the Wilson method (*5*):

$$P_{error} = P \pm \frac{1.96 n^{1/2}}{(n + 1.96^2)} (P(1-P) + (1.96^2/(4n)))^{1/2} \tag{3}$$

By inserting P_{error} into (2) confidence intervals for τ are obtained. Note that the final error bars for τ shown in Figure 5 of the paper include the uncertainty in $t_0 \in [50, 150]$.

2 Supporting Figures

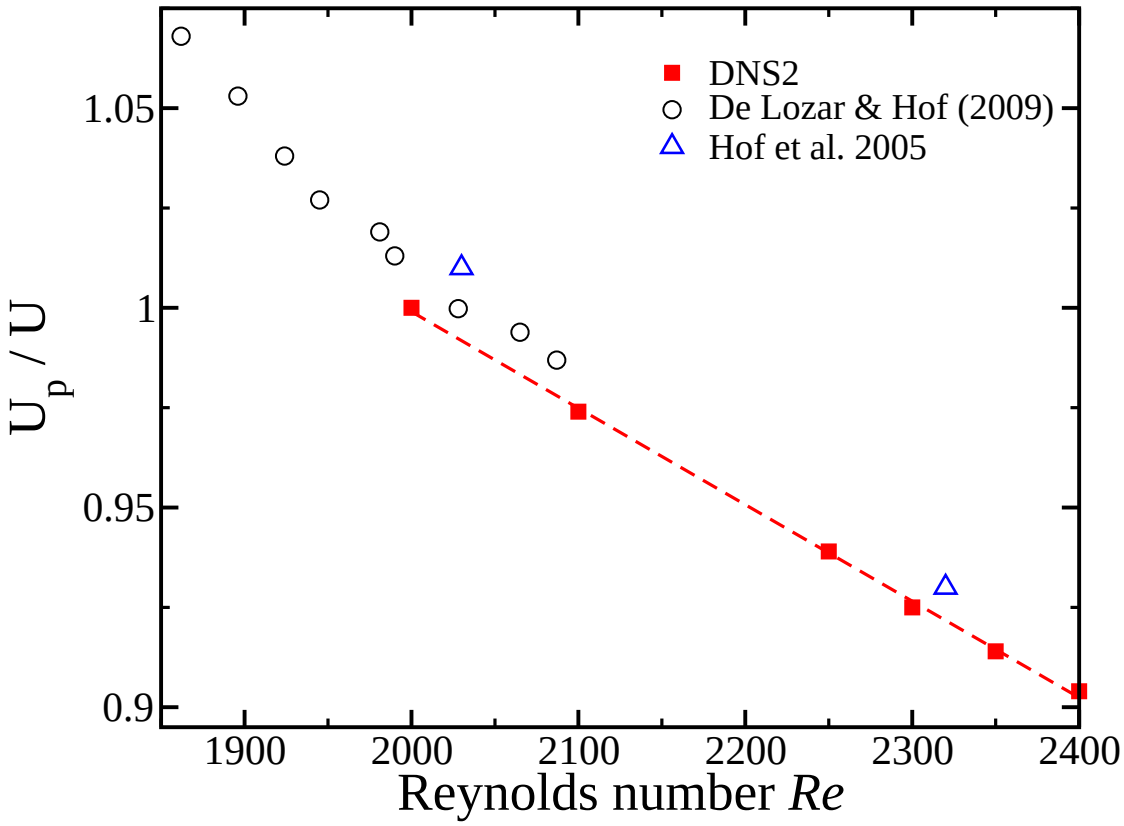

Figure S 2: Numerically computed puff speed (squares) using the hybrid spectral finite-difference code. The puff speed is very well approximated by Eq. S1 over the range $2000 \leq Re \leq 2400$ plotted as red dashed line. Circles are from experiments in (*6*) and triangles from (*7*).

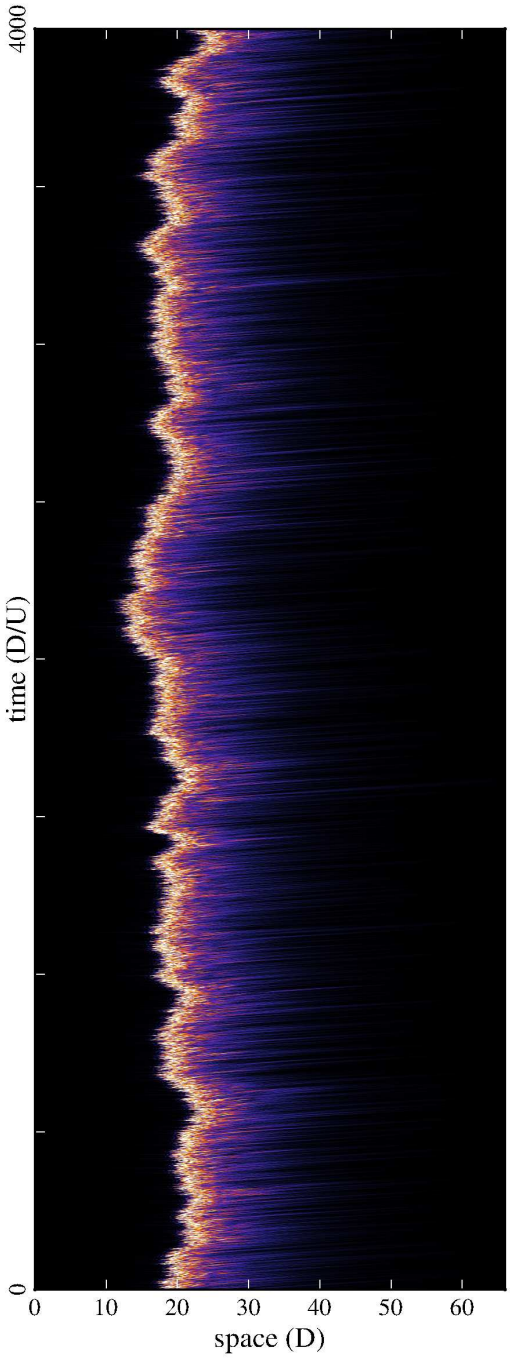

Figure S 3: Space-time diagram for a puff at the critical Reynolds number $Re = 2040$. Streamwise vorticity is plotted on a linear scale in a co-moving reference frame (speed $U_p = 0.9873U$ from Eq. S1). There are fluctuations in the width and intensity, but on the whole the size and speed of a puff at this *Re* is constant, i.e. it is an 'equilibrium puff' (*8*). Based on the evidence presented in the paper, the puff will eventually, with nearly equal probability, decay or split. However, the characteristic time for this to occur is more than $10^7 D/U$, considerably longer than the 4×10^3 D/U shown here.

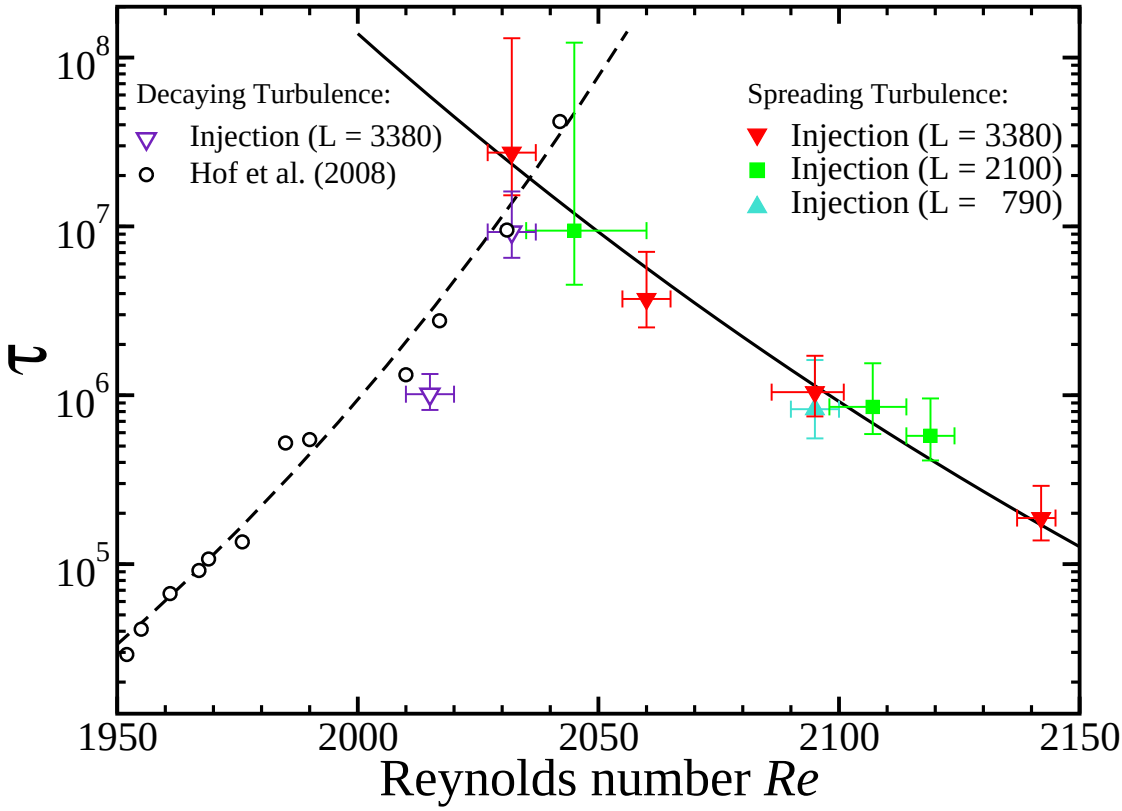

Figure S 4: Enlargement of Fig. 5 in the vicinity of the critical point.

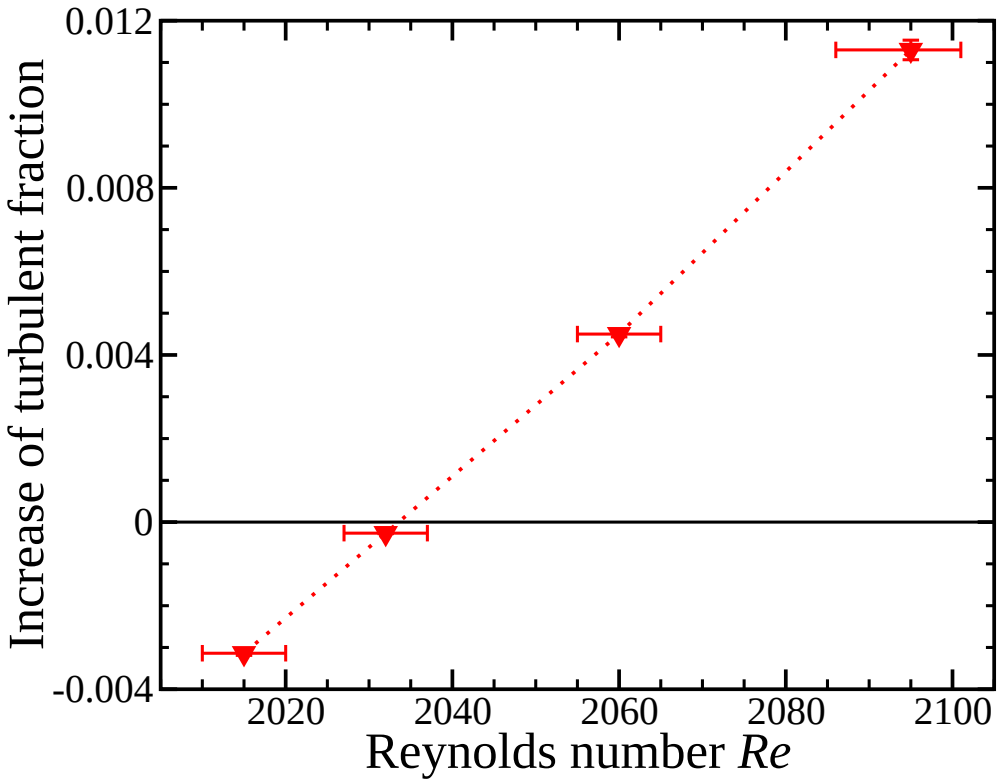

Figure S 5: Increase of the turbulent fraction from experimental measurements defined as $I = (S_{3380} - S_{puff})/S_{puff}$. At each *Re* the size of the turbulent region is measured at a distance of $L = 3380$ from the perturbation by setting a threshold on the pressure signal (see also Fig. S1 (B)). The measurement is subsequently repeated to determine the average turbulent size (S_{3380}). Finally, the value is normalized with respect to the mean size of a single puff (S_{puff}) measured at this *Re* using the same threshold. The dotted line connects measurements to guide the eyes. Below the critical point $Re_c \simeq 2040$ the turbulent fraction decreases, as indicated by negative values of I, whereas for supercritical *Re* it increases. The error bars in the vertical direction are 95% confidence intervals of the increase of the turbulent fraction. Note, that they are hidden by the symbol in most of the cases. The size of a single puff is here about $S_{puff} \approx 25D \pm 10D$.

3 Supporting Table

Table S 1: Tabular data for Fig. 5. (Experiment) Characteristic splitting time τ from experiment (jet perturbation) as a function of Reynolds number *Re* and $t_0 = 100$. Each row corresponds to a set of measurements. The fourth and fifth columns indicate the number of splitting events *r* and total number of runs *n*.

L	*Re*	τ	*r*	*n*
350	2252	2735	21	221
	2273	1801	99	699
	2295	1062	415	1806
	2333	663	144	417
790	2095	826518	17	19844
	2173	33776	22	1037
	2252	3817	39	221
	2273	2080	451	1497
	2295	1240	1302	2868
	2333	673	282	417
	2379	404	3600	4229
1664	2199	17702	76	854
	2237	6633	54	243
	2277	2238	182	344
	2308	1274	123	167
	2327	861	583	676
	2351	642	922	990
2100	2045	9434617	4	18636
	2107	852816	20	8298
	2119	574935	25	6975
	2170	48717	156	3711
	2237	6721	66	243
	2253	4777	61	169
	2277	2357	206	344
	2308	1216	139	167
	2324	778	635	676
	2351	548	972	990
	2385	485	960	970

L	*Re*	τ	*r*	*n*
3380	2032	27338718	7	57823
	2060	3715436	18	20073
	2095	1042648	26	8074
	2142	187364	31	1722
	2185	49835	66	989
	2201	25358	178	1397
	2212	19142	160	966
	2239	7525	366	986
	2253	5896	2666	5950
	2269	3728	1562	2557
	2283	2830	4226	5928
	2305	1654	1029	1165
	2325	975	1825	1873
Obstacle				
1700	2214	9719	8	50
	2285	1691	32	50

Table S 2: Tabular data for Fig. 5. (Lifetime) Characteristic decay time τ from experiment (jet perturbation) as a function of Reynolds number *Re* and $t_0 = 0$. Each row corresponds to a set of measurements. The fourth and fifth columns indicate the number of decaying events *r* and total number of runs *n*.

L	Re	τ	r	n
3380	2015	1014588	67	20052
	2032	9262569	22	59773

Table S 3: Tabular data for Fig. 5. (DNS) Characteristic splitting time τ from direct numerical simulations as a function of Reynolds number *Re*. The second and third columns indicate the number of splitting events *r* and total number of runs *n*. The runs were terminated after registering a splitting or after a truncation time of $t_{\max}$. The earliest splitting time for a set of runs is indicated as t_1. Upper and lower confidence intervals $\pm\Delta\tau$ are given in columns 7 and 8, respectively are are generated using $B = 10^5$ bootstrap samples.

	Re	τ	r	n	t_1	$t_{\max}$	$+\Delta\tau$	$-\Delta\tau$
DNS1	2275	1795	15	30	281	1500	1349	664
	2300	1042	22	30	177	1500	550	344
	2325	563	27	30	233	1500	247	184
	2350	445	48	50	170	1500	133	109
	2375	454	29	30	147	1500	153	116
DNS2	2250	5696	12	50	410	2000	6465	2269
	2300	1923	29	60	194	1500	965	572
	2350	484	42	45	130	1500	165	130

References

1. H. M. Blackburn, S. J. Sherwin, *J. Comput. Phys.* **197**, 759 (2004).

2. A. P. Willis, R. R. Kerswell, *J. Fluid Mech.* **619**, 213 (2009).

3. M. Avila, A. Willis, B. Hof, *J. Fluid Mech.* **646**, 127 (2010).

4. J. Lawless, *Statistical Models and Methods for Lifetime Data* (Wiley, New Jersey, 2003), second edn.

5. L. D. Brown, T. T. Cai, A. DasGupta, *Stat. Science* **16**, 101 (2001).

6. A. de Lozar, B. Hof, *Phil. Trans. Roy. Soc. Lond. A* **367**, 589 (2009).

7. B. Hof, C. W. H. van Doorne, J. Westerweel, F. T. M. Nieuwstadt, *Phys. Rev. Lett.* **95**, 214502 (2005).

8. I. Wygnanski, M. Sokolov, D. Friedman, *J. Fluid Mech.* **69**, 283 (1975).